Article:
Yang, K orcid.org/0000-0002-4223-2710, Yang, Y, Deng, J et al. (5 more authors) (2022) Using calcium-rich precursors to improve the early-compressive strength of alkali-activated slag cement at low temperature. Structural Concrete, 23 (4). pp. 2221-2232. ISSN 1464-4177

https://doi.org/10.1002/suco.202100021

Using calcium-rich precursors to improve the early-compressive strength of alkali-activated slag cement at low temperature

Kai Yang[a,b], Yong Yang[a,c], Jiaxin Deng[a], Deyi Xiong[a], **Xiaohong Zhu**[a,b*], Qing Li[d], Changhui Yang[a], Muhammed Basheer[b]

a: College of materials science and engineering, Chongqing University, Chongqing, China
b: School of civil engineering, University of Leeds, Leeds, UK
c: Sichuan institute of building research, Chengdu, China
d: College of Civil and Architectural Engineering, Guilin University of Technology, China

Corresponding author: Xiaohong Zhu (cnxz@leeds.ac.uk)

Abstract:
This study examines the potential of using calcium-rich precursors to improve the strength of alkali-activated slag (AAS) cement at low temperature. To achieve this target, the effect of calcium-rich precursors on the early strength development of AAS mortars cured at 5 ºC was assessed. The strength development was investigated along with its internal temperature, microstructure and reaction products. It is found that the calcium-rich precursors can improve the early strength of AAS around 35% and the group with Portland cement clinker gave the highest strength. Calcium oxide (CO) can also increase the compressive strength of AAS cement, but its effectiveness is not as good as the sample with clinker. Adding calcium sulphoaluminate (CSA) can increase the early strength, while no significant contribution to 28-d strength could be found. The results highlight that compressive strength of modified AAS mortar can reach 15 MPa at 6 hour and 20 MPa at 24 hour at 5 ºC, suggesting that the this binder could be a valuable alternative for low temperature construction.

Keywords: alkali-activated slag, low temperature curing, reaction product, microstructure

1 Introduction

Developing high-performance binding materials for construction at low temperature attracts special attention in the cold region. For example, winter in northern China lasts for 6 months and the outside temperature is generally lower than 5ºC and under such low temperature, conventional Portland cement suffers from the slow hydration rate, long setting time and low early strength [1-3], e.g. the 1-d compressive strength of mortars cured at 5 ºC for was less than 5 MPa [3,4]. A range of techniques, e.g. nano-materials [5], antifreeze and early strength admixtures [6], have been used to improve early strength development of Portland cement at low temperature through physical or chemical mechanisms, the performance-cost ratio of these approaches is not as high as expected. Calcium sulphoaluminate (CSA) cement has shown excellent mechanical performance and the compressive strength of CSA mortar could exceed 20 MPa at 5 ºC for 1 d [7]. However, the availability of CSA is limited at some regions. Consequently, searching for high strength and rapid setting cements is an important task for civil engineers.

Alkali-activated slag (AAS) cement that is prepared by alkali activator and ground granulated blast furnace slag (GGBFS) receives intense attentions recently due to the use of industrial by-products to reduce CO_2 emission [8,9]. Numerous studies have shown outstanding performances of AAS cement, such as high strength, rapid strength development. In addition, the high ionic concentration of the alkaline solution could enable slag to continue react in low or negative temperature environment [10,11]. These characteristics suggest that AAS cement has a great potential in construction under low

temperature [12]. However, mechanical properties of AAS cement are very sensitive to curing temperature [13-15] and nearly no consistent trends can be found. Gu et al. [16] and Du et al [17] reported that the early reaction rate of AAS at low temperature (5-7 ^{o}C) was slow, but the compressive strength of mortar cured for 3 d at 7 ^{o}C reached 18.4 MPa. Samantasinghar and Singh [18] and Li et al [20] also stated that when the slag was activated with NaOH, the reaction rate of slag at the early age at low temperature was slow, especially for low alkali (pH ≤13.02) dosage.

Very few literature on improvement of the early strength of AAS cement at low temperature has been reported, although numerous studies examine early mechanical properties of AAS at room temperature. For example, Gao et al. [20] and Xiang et al [21] reported that fine limestone powder cannot only give a physical filling effect, but also provide additional nucleation sites for reaction products, which is beneficial for early strength development of AAS; Cheng et al [22] found that the early strength of AAS without adding $Ca(OH)_2$ was much lower than that of $Ca(OH)_2$-added sample; Temuujin et al [23] indicated that CaO and $Ca(OH)_2$ can react with water glass to form amorphous substances or poorly crystalline C(-A)-S-H gel. Experiments from Lee and Van-Deventer [24] showed that Ca salts can provide heterogeneous nucleation centers in the solution, managed ionic contamination can improve the early strength of AAS. Jeong et al [25] also indicated that Ca-based materials have better effects on the strength of AAS. These studies suggest that the addition of calcium-rich precursors to high calcium fly ash-based materials will accelerate the growth of compressive strength of AAS cement [23,26]. Currently, there are few studies on the influence of calcium-rich precusors on the early strength of AAS under low temperature environment, especially for the strength development within 24 h. As such, features of strength development of AAS cement under low temperature need to be examined and techniques of improving its performance should be investigated to assess its potential as a rapid repairing material.

This work selected water glass as an activator to investigate the effect of common calcium-rich precursors on the early strength development of AAS at low temperature (5 ^{o}C). Multi technologies, including internal temperature, X-ray diffraction (XRD), thermogravimetric analysis (TGA), mercury intrusion porosimetry (MIP) and backscattered electron image (BSE), were used to examine impacts of calcium-rich materials on reaction products and early microstructure evolution of AAS cements.

2 Materials and methods

2.1 Raw materials

Ground granulated blast-furnace slag (GGBS) was provided by Chongqing Iron and Steel Group. The measured density and specific surface area of GGBS are 2.91 g/cm^3 and 430 m^2/kg. Its alkalinity coefficient is 0.99. Portland cement clinker (PC) was produced by Chongqing Tianzhu Cement Plant, which came as lumps. Before using the clinker in the mix, it was grounded for 30 mins in the ball mill and its density is 3.10 g/cm^3 with specific surface area of 330 m^2/kg. Calcium sulphoaluminate cement (CSA, grade 82.5) came from Tangshan Polar Bear Building Materials Co., Ltd. Its density and specific surface area are 3.06 g/cm^3 and 410 m^2/kg. The chemical compositions of the three binders, GGBS, clinker and CSA, were determined by XRF, the results of which are summarised in **Table 1**.

Four calcium-based supplementary materials were selected to examine their influences on the strength development of AAS cement at low temperature. Calcium hydroxide is labeled as CH, the content of $Ca(OH)_2$ ≥95.0%, calcium oxide is labeled as CO, the content of CaO ≥98.0% and calcium chloride anhydrous is labeled as CCl, the content of $CaCl_2$ ≥96.0%. The three admixtures were analytical purity (AR). The fourth precursor is limestone powder (labeled as CC, the content of $CaCO_3$ ≥98%) and its specific surface area and average particle size are 2120 m^2/kg and 3.2 μm.

Industrial grade liquid sodium silicate (water glass), composed of 30.20 wt% SiO_2, 12.24 wt% Na_2O and 46.53wt% H_2O, was used as the alkaline activator. The modulus of water glass was adjusted to 2.0 ($n=SiO_2/Na_2O$) by NaOH. The content of alkali was 8% by mass of slag (Na_2O equivalent).

Natural sand with a fineness modulus of 2.50 was used to manufacture mortar samples.

2.2 Sample preparation and curing regime

Calcium-rich precursor was used to replace the GGBFS and two levels were considered at first. In total, 13 mixes were manufactured, the mix proportions of which are given in **Table 2**. Two types of specimens were prepared, cement paste samples for assessing reaction process and microstructure characteristics, and mortar samples for determining mechanical strength. The water-binder ratio (W/B) of all mixes was kept as a constant, 0.35, and the water in the alkali solution was considered as free water to calculate the W/B. The binder-sand ratio (B/S) of the mortars was 1:1.5 to achieve high early strength [32].

The alkali activator solution was prepared 1 d before mixing, sealed with plastic film to prevent moisture loss and placed in a room at a constant temperature of 20 ± 2 ºC. The moulds and other raw materials were placed in a container at 5 ± 2 ºC for 1 day before mixing. It should be noted that the mixing process was carried out in a room temperature of 20 ± 2 ºC in 3 minutes.

Calcium-rich supplementary material was added during the mixing process. Two sets of mortar samples with the dimensions of 40 × 40× 40 mm^3 were prepared for each mix. They were moved into a low temperature container for curing immediately after casting. After 6 hours, samples were removed from moulds and placed in the 5 ºC container until 24 hours. All mixes in **Table 2** were used in testing the early strength cured at 6 h and 24 h. Paste samples (20 × 20 × 20 mm^3) were prepared under the same procedure and they were used in monitoring internal temperature change, XRD, TGA, MIP and BSE tests. Detailed experimental programme was summarised in **Table 3**.

2.3 Test methods

2.3.1 Compressive strength

Compressive strength of AAS mortar samples (40× 40× 40 mm^3) was tested according to the Chinese National Standard GB/T 17671-1999: Cement mortar strength test [27] at the age of 6 h, 24 h, 3 d, and 28 d. The samples were removed from the 5 ºC curing chamber and strength measurements were carried out within 10 mins. The average value of 3 samples was recorded as the reported strength.

2.3.2 Temperature inside paste sample

To examine the influence of calcium-rich precursors on the exothermic process of AAS, the internal temperature change of paste samples was monitored using the embedded temperature sensor, DS18B20 (-55 to +125 °C ±0.5°C, Maxim, USA). The mould was made of polystyrene foam boards with a thickness of 30 mm for 100 ×100 ×100 mm^3 size. The temperature sensors were placed in the center of mould immediately after casting and the samples were covered with polystyrene foam board in order to reduce loss of heat. Temperature was recorded at an interval of 1 minute for 24 hours.

2.3.3 X-ray diffraction (XRD)

The AAS paste samples (curing for 6 hours and 28 days) were crushed and its reaction was stopped by the solvent-exchanged method using ethanol, followed by vacuum drying at 40 °C for 3 days. After this, the samples were ground and sieved through a 200-mesh sieve to obtain powders. The XRD measurements were carried out using the D/Max-5A12kW X-ray diffractometer (40kV and 40mA) with Cu Kα radiation (Rigaku, Japan), the scanning speed was 4 º/min, and the scanning range is 5º ~ 90º (2θ).

145
146 2.3.4 Thermogravimetric analysis (TGA)
147 Powder samples obtained by the method described above were also used for TGA tests. The 1600LF
148 thermogravimetric differential thermal synchronous thermal analyzer (Mettler Toledo, Switzerland)
149 was used to monitor the weight change. The test temperature range was 30-1000 ºC in a N_2
150 environment and the heating rate was 20 ºC/min.
151
152 2.3.5 Mercury intrusion porosimetry (MIP)
153 At the age of 6 hours and 28 days, the paste samples were crushed to particles with size of 3–5 mm to
154 avoid additional pore volume entrapment by the size effect during MIP. The samples were then
155 immersed in the solvent for 3 days to stop reactions, followed by vacuum drying at 40 °C until constant
156 weight was reached. The pore size distribution and porosity were determined by Auto Pore IV9500
157 (Micromeritics, USA) and the effective pore size range was 3 nm-350 μm.
158
159 2.3.6 Backscattered electron images (BSE)
160 Paste samples (curing for 6 hours) obtained by the method described in 2.3.5 were vacuum
161 impregnated with epoxy-resin. After the epoxy-resin was completely hardened, the samples were
162 polished successively with different mesh of sandpaper (400, 600, 1000, 2000, 3000, 4000 mesh) until
163 a smooth surface was obtained and then coated with gold. Finally, the samples were examined by field
164 emission scanning electron microscopy (SEM, NOVA 400, FEI, USA) using backscattered electron
165 mode (BSE) with an acceleration voltage of 18kV.

166 **3 Results and discussion**

167 **3.1 Compressive strength**
168 **Fig. 1** shows the influence of clinker (PC), CSA, $Ca(OH)_2$, limestone, CaO and $CaCl_2$ on the early
169 compressive strength development of AAS mortar curing for 6 h and 24 h at 5 ºC. It is shown that the
170 early compressive strength of all samples was more than 10 MPa, which indicates that AAS binder has
171 a great potential for practical applications at low temperature. Meanwhile, calcium-rich precursors can
172 improve the early compressive strength of AAS mortar, whilst their effect depends on the type and
173 dosages.
174
175 From **Fig.1**, AAS-15%PC (clinker: 15%) exhibited the highest strength, where the compressive
176 strength of the mortar at 6 h and 24 h increased by 35% and 43%, respectively. This would be attributed
177 to two reasons. Firstly, the clinker can work as an activator [28], which can improve the reactivity of
178 GGBFS and promote its decomposition. The other reason is that clinker reacted rapidly and produced
179 more reaction products, especially in high alkaline solution. The addition of 12%CSA also showed a
180 similar feature due to the fast reaction of CSA in high alkaline solution. However, the effect was not
181 obvious when the dosage was low. The above results indicated that using a proper amount of calcium-
182 rich precursors to replace GGBFS can bring a beneficial effect on development of mechanical strength.
183
184 As GGBFS was replaced by the calcium-rich precursors, two effects have been identified, physically
185 filling effect and additional chemical reactions with activator and/or GGBFS. The extent of the
186 influences depends on several factors. When limestone powder ($CaCO_3$) was added into the mixes, the
187 growth of compressive strength was observed at the low level (7.5%), while the contribution is not
188 clear at the high level (15%), suggesting that the early strength does not increase with the increase of
189 the dosage. Gao et al. [20] pointed out that fine limestone powder can accelerate reaction of AAS
190 cement, because limestone powders provide additional nucleation sites and the small particles also can
191 fill the pores [21]. However, this impact disappears as the dosage increases. The main reason is that
192 replacing GGBFS by too many inactive powders would increase the distances between GGBFS

particles, making connections between reaction products more difficult.

In addition to the filler effect, calcium hydroxide ($Ca(OH)_2$) and calcium oxide (CaO) can react with alkali-solution and GGBFS to form amorphous materials or poorly crystalline C-(A)-S-H gels [23,29]. According to results in **Fig. 1**, addition of $Ca(OH)_2$ in the range between 2.5 and 5% can give a gentle improvement in compressive strength, while its amount does not play a significant role. For a given dosage, CaO would be able to increase strength further. This trend becomes quite clear when 5% of CaO was added in the mix. This feature is due to additional heat during dissolution of CaO to form $Ca(OH)_2$ [30]. The results also highlight that $Ca(OH)_2$ may provide some Ca^{2+} in the alkali-solution that could react with silicate ion provided by water glass [29], while this contribution is not significant due to its low solubility. The calcium chloride ($CaCl_2$) is able to improve compressive strength, while this feature can be seen only at the low level of dosage. It is well known that $CaCl_2$ can accelerate the reaction process of AAS cement at the early age through heterogeneous nucleation and crystallisation [23,24]. However, the opposite trend is found in **Fig.1**, when the dosage of $CaCl_2$ is above 0.25%. This means that inorganic Ca salts was active in promoting polymerisation, but the high dosage of $CaCl_2$ may cause retarding [24], which is not good to the growth of early strength.

According to the results obtained, some calcium-rich precursors were selected to further explore their influence on the strength development of AAS mortar at 28 days, and the calcium sulphoaluminate cement mortar (Pure-CSA) with the water-binder ratio (W/B = 0.35) was also selected as the reference sample for comparison. It is clear in **Fig.2** that for a given W/B ratio and under the same curing conditions, the compressive strength of Pure-CSA at 6 h is the lowest in all mixes examined, while its 1 d and 3 d strength of was the highest. The results highlight the fact that AAS mortars perform better for the first 6 h and its strength can be further improved by adding suitable calcium-rich precursors, so it is able to meet requirements of high early strength in rush repair and construction projects. Meanwhile, among these calcium-rich precursors, the clinker seems to give the best performance, while CaO can also improve the 28-d strength, before which no significant difference could be found. A similar result about CSA was reported by Jia et al [31], who found that 12% CSAE (calcium sulphoaluminate type expansion agent) had no effect on the 28-d strength of AAS mortar.

3.2 Internal temperature change

The variation of internal temperature in paste samples is plotted in **Fig. 3**. Clearly, the internal temperature rose rapidly after mixing due to the high alkaline environment (8% alkali concentration), which is helpful to promote the dissolution of slag particles [32] and accelerate the rate of heat release. Meanwhile, the temperature curve of all samples has one exothermic peak, similar to results reported in previous reports [32]. Although the peak of the internal temperature is different for each mix, all exothermic peak appear around 150 mins. It indicates that addition of calcium-rich precursors can affect the reaction rate of AAS mixes, while would not significantly change the duration of heat release. More specifically, the internal temperature of the AAS-15%PC and AAS-5%CO grew much faster than that of other AAS mixes. As the time to reach the highest internal temperature for these mixes was almost the same, the greatest difference in temperature arrived at that point, which varies from 25-30 ^{o}C. The additional temperature rise can be explained by heat release related to chemical reactions of PC clinker and heat of dissolution induced by dissolving CaO, respectively. Higher temperature is beneficial for accelerating chemical reactions and these results are clearly linked with rapid increases in compressive strength for AAS-15%PC and AAS-5%CO.

Fig. 3 also shows the temperature curve of calcium sulphoaluminate cement system (Pure-CSA). It can be found that the temperature started rising after 200 minutes and reached the peak value around 350 minutes. This demonstrates that the early reaction rate (especially in the first 3 hours) of the AAS pastes were faster than that of Pure-CSA sample and the reaction heat released in early stage was higher,

but temperature in the CSA system was higher than AAS between 300 to 600 minutes. This can explain why for Pure-CSA, compressive strength at 6 hours (360 minutes) was relatively low, while the opposite trend was observed at 1 day (1440 minutes).

3.3 X-ray diffraction (XRD)

Fig.4 shows the XRD patterns of paste samples examined in this study. According to the peak identified, the primary reaction product at 6 h and 28 d of all mixes are C-(A)-S-H gel (around 30^o (2θ)), which agrees with results given in previous research studies [33,34]. Meanwhile, the peak around 30^o (2θ) is sharp with a high intensity for mixes with calcium-rich precursors. This indicates that the features of C-(A)-S-H gel might be changed, which could be due to the increase in the Ca/Si ratio [35,36]. In addition, the characteristic peak of gehlenite in slag is obvious at 6 h and 28 d. Similar to results presented by Ben-Haha et al. [33] and Kim et al. [37], the degree of reaction of GGBFS was relatively low, especially in low temperature.

As shown in **Fig. 4-a**, new phases were found at 6 h from the samples with calcium-rich precursors for AAS-15%PC, C_2ASH_8 and C_4AH_{13}. Yang et al. [38] reported that these high calcium products were tightly absorbed by C-(A)-S-H gel with a higher Ca/Al ratio and this could relate to the higher strength development of mortar. In addition to the unreacted ye'elimite phase ($Ca_4Al_6O_{12}SO_4$) at 6 h, $Al(OH)_3$ crystals were formed from AAS-12% CSA, but no ettringite was found. This differs from the results of Jia et al. [31] used SEM to find ettringite was produced from the AAS sample with the addition of calcium sulphoaluminate type expansion agent. The differences of these results probably relate to the liquid phase, curing temperature and the sulphate content from raw materials and a high sulphate content might favour the formation of ettringite [25,39]. Meanwhile, the $CaSiO_3$ was detected in AAS samples with addition of CaO or $CaCl_2$, as a result of the reaction between Ca^{2+} from calcium salts and silicate ion from the water glass solution [40].

New phases found at 24 h were gradually consumed except for C_4AH_{13} as the age increases, for example, $Ca(OH)_2$ can participate to form other reaction products or carbonates to form calcium carbonate during sample preparation [41]. This implies that the four calcium-rich precursors would not change the type of reaction products in AAS samples.

3.4 Thermogravimetric analysis (TGA)

The results of thermogravimetric analysis are given in **Fig. 5**. For all samples, a distinct mass loss occurs at 90 ºC from DTG curves, which is caused by dehydration of C-(A)-S-H gel. It is noticed that the temperature of its peak is slightly low compared with results given in previous studies [35,42]. Low temperature curing led to the rapid mass loss that was mainly from the loss of bound water. The trend indicates that low temperature curing may weaken the ability of bonding water of C-(A)-S-H gel.

After removing the free moisture, the mass loss below 250 ºC correlates well with the amount of C-(A)-S-H gel in the AAS system [35,41,43]. As shown in **Fig.5-a**, the mass loss of AAS-15%PC sample cured at 6 h is the highest at this region (10.71%), which provides direct evidence for its trend on compressive strength. Unsurprisingly, the mass loss of AAS-15%PC and AAS-5%CO samples at 28 d are higher than that of the control group that links with its high compressive strength (as shown in **Fig. 2**). It is also noticed that the mass loss of AAS-12%CSA or AAS-0.25%CCl samples were almost equal to the AAS (control) sample from 6 hours to 28days, which implies that the addition of CSA or $CaCl_2$ could not increase of the amount of reaction products.

The DTG curve of AAS-5%CO shows noticeable endothermic peaks in the range of 400-450 ºC and 580-650 ºC, which would be due to decomposition of $Ca(OH)_2$ [41,42] generated by CaO reacted with water and decomposition of $CaCO_3$ with low crystallinity [46], respectively. Calcites in these mixes

decomposed between 750-800 ºC [41,42,44], and the mass loss was more visible at 28 day for carbonisation. These products corresponding to the different temperature interval of mass loss from TG/DTG results agree well with XRD data.

3.5 Mercury intrusion porosimetry (MIP)

The strength of cement-based materials is a function of the porosity and pore size distribution [10,15]. To examine the influence of calcium-rich precursors on strength of AAS cement at low temperature, the porosity and pore size distribution of AAS pastes were determined using MIP. **Table 4** and **Fig. 6** summarise the pore size distribution ratio and total porosity of samples. It is clear from **Table 4** that most pores in nearly all samples, more than 80%, were smaller than 30 nm after 6-hour curing at 5 ºC. Similar results have been reported by Gu et al. [15] and Collins et al. [45]. It might be concluded that the pore size distribution of AAS might not be strongly affected by the curing temperature. In addition, the pore size of each sample was fine and located at a narrow region, and the pore structure was uniform at the age of 28 day.

Addition of four calcium-rich precursors mainly affects the fine pore (d <10 nm) ratio in AAS samples at 6 h. The fine porosity (total porosity × ratio of fine pores) of the AAS-0.25%CCl and AAS-12%CSA samples is lower than the control group, while the TG results indicate that the amount of C-(A)-S-H gel at 6 h are similar to the control group. This probably means that the density of the C-(A)-S-H gel layer of AAS after incorporation of $CaCl_2$ or CSA was higher than pure AAS sample. Besides, for AAS-5%CO sample, the ratio of pores between 10-30 nm is lower than other mixes, while there are more macropores and air pores with diameter greater than 30 nm. This may be due to the high water demand of CaO (some water was consumed by CaO in the process of forming $Ca(OH)_2$), which can lead to the decrease of the fluidity of paste and more macropores and air pores were introduced by stirring. Hence, more coarse pores were found in AAS-5%CO.

It is clear that the 6 h total porosity of AAS after blending with clinker, CSA, CaO, and $CaCl_2$ are lower than that of the control sample (shown in **Fig.6**), while the low porosity was beneficial for obtaining high compressive strength [10] and it is in agreement with high early strength results. Among them, adding clinker can significantly reduce the porosity of 6 h. Except for AAS-15%PC, the total porosity of other three mixes stay quite close to the control at the age of 28 day, meaning that they mainly affect the early age strength and no significant improvements are found beyond 28 days.

3.6 Backscattered electron image (BSE)

Fig. 7 and **Fig. 8** compare the backscattered electron (BSE) images of five mixes that were taken at 6 h and 28 d. Three phases can be identified in these BSE images, including bright unreacted clinker/GGBFS particles, dark reaction products and black pores, e.g. highlighted in **Fig.7-a**. As shown, there are numerous unreacted fine particles in each sample after 6 hours, and the angular unreacted particles were randomly distributed in the matrix formed by reaction products. It indicates that the early reaction degree of samples is very low. Meanwhile, there are a few pores above the micron level that can be seen from BSE images, which are close to the MIP results. The appearance of these macropores is not good to improving the early strength. In addition, it is not easy to distinguish the calcium hydroxide from BSE images. Gray difference is not found in the region products around the slag particles after adding calcium-rich material from **Fig. 7** and **Fig. 8**. This may be because the reaction products have sufficient time to diffuse throughout the matrix and precipitate uniformly at low temperature [46].

Fig. 7- a and **c** show that the layer of reaction products in AAS-15%PC and AAS-5%CO is thicker than others. Meanwhile, the products are uniform, but there are more microcracks in these two samples. The microcracks were found in regions of reaction products (grey areas). The significant difference in

temperature at early reaction for the AAS pastes mixed with PC clinker or CaO can cause large thermal stress. The drying process in sample preparation that would also produce drying shrinkage stress, leading to cracks [41]. Moreover, black areas were found in the samples of AAS-12%CSA and AAS-0.25%CCl and it is the remaining water-filled space after reaction, and these spaces will be filled with reaction products and reduce as age goes (as shown in **Fig. 7- b** and **d**). Similar trends were found in **Fig. 8**, except for less unreacted tiny slag particles found due to continuous reaction. This result showed that the reaction degree of slag significantly improved at the later stage even under low temperature.

4 Conclusion

The influence of common calcium-rich materials on the early strength development of AAS mortar cured at low temperature (5 ^{o}C) was studied. Based on results obtained, the following conclusions can be drawn:

1) Under low temperature environment, adding suitable amount of calcium-rich materials to AAS system can improve the early strength of mortar effectively. The use of PC clinker or CaO can promote 28 d compressive strength of AAS mortar, while CSA and $CaCl_2$ have no negative impact on the later age. The strength of modified AAS mortar can reach 15.8 and 22.1 MPa at 6 hour and 24 hour respectively.
2) The addition of PC clinker or CaO could increase the early internal temperature and accelerate the heat release rate of AAS system in the initial 10 hours, while the exothermic process of AAS would not be changed by adding calcium-rich materials.
3) C_2ASH_8 and C_4AH_{13} were found in AAS paste mixed with PC clinker at the age of 6 h from XRD result. Meanwhile, $CaSiO_3$ was found in samples with CaO or $CaCl_2$, but no new phase was detected after 28 days. The TD/DTG results showed that adding 15% clinker could significantly increase the amount of C-(A)-S-H gel in the sample.
4) Clinker, CSA, CaO and $CaCl_2$ can reduce the total porosity of AAS in the early stage, increase the thickness of the hydration product layer, improve the microstructure, which are beneficial to the early strength development.
5) Adding calcium materials like clinker and CSA in AAS can exert chemical effects, while fine $Ca(OH)_2$ and limestone powder also can exert micro filling effects, these technical approaches are useful to improve the early strength of AAS in low temperature environments.

These results indicate that the modified AAS cement could be considered as a potential rapid repairing material, while further investigation on long-term performance, e.g. aging and durability, should be examined before practical applications.

Acknowledgments

The authors are grateful to these funding for providing financial support: National Natural Science Foundation of China (NO. 51878102), National Key R&D Program of China (No. 2017YFB0309905), Analytical and Testing Center of Chongqing University. In addition, supports provided from University of Leeds during analysis of data and preparation of this paper are also highly appreciated.

Data availability

The data that support the findings of this study are available from the corresponding author upon reasonable request.

References

[1] Escalante-Garcıa J I, Sharp J H. The microstructure and mechanical properties of blended cements hydrated at various temperatures[J]. Cement and Concrete Research, 2001, 31(5): 695-702.

[2] Kjellsen K O, Detwiler R J. Reaction kinetics of Portland cement mortars hydrated at different temperatures[J]. Cement and Concrete Research, 1992, 22(1): 112-120.

[3] Lothenbach B, Winnefeld F, Alder C, et al. Effect of temperature on the pore solution, microstructure and hydration products of Portland cement pastes[J]. Cement and Concrete Research, 2007, 37(4): 483-491.

[4] Xu L, Wang P, Zhang G. Formation of ettringite in Portland cement/calcium aluminate cement/calcium sulfate ternary system hydrates at lower temperatures[J]. Construction and Building Materials, 2012, 31: 347-352.
[5] Xu Q L, Meng T, Huang M Z. Effects of nano-$CaCO_3$ on the compressive strength and microstructure of high strength concrete in different curing temperature[C], Applied Mechanics and Materials. Trans Tech Publications, 2012, 121: 126-131.
[6] Richardson A. Strength development of plain concrete compared to concrete with a non-chloride accelerating admixture[J]. Structural survey, 2007, 25(5): 418-423.
[7] Wang P, Li N, Xu L. Hydration evolution and compressive strength of calcium sulphoaluminate cement constantly cured over the temperature range of 0 to 80 ^{o}C [J]. Cement and Concrete Research, 2017, 100: 203-213.
[8] Li Q, Yang Y, Yang K, et al. The role of calcium stearate on regulating activation to form stable, uniform and flawless reaction products in alkali-activated slag cement [J]. Cement and Concrete Composites, 2019, 103: 242-251.
[9] Myers R J, Bernal S A, Provis J L. Phase diagrams for alkali-activated slag binders [J]. Cement and Concrete Research, 2017, 95: 30-38.
[10] Shi C. Strength, pore structure and permeability of alkali-activated slag mortars[J]. Cement and Concrete Research, 1996, 26(12): 1789-1799.
[11] Bakharev T, Sanjayan J G, Cheng Y B. Effect of elevated temperature curing on properties of alkali-activated slag concrete[J]. Cement and concrete research, 1999, 29(10): 1619-1625.
[12] Yang K, Yang C, Zhang J, et al. First structural use of site-cast, alkali-activated slag concrete in China[J]. Proceedings of the Institution of Civil Engineers-Structures and Buildings, 2018, 171(10): 800-809.
[13] Wang S D, Scrivener K L, Pratt P L. Factors affecting the strength of alkali-activated slag[J]. Cement and concrete research, 1994, 24(6): 1033-1043.
[14] Živica V. Effects of type and dosage of alkaline activator and temperature on the properties of alkali-activated slag mixtures[J]. Construction and Building Materials, 2007, 21(7): 1463-1469.
[15] Altan E, Erdoğan S T. Alkali activation of a slag at ambient and elevated temperatures[J]. Cement and Concrete Composites, 2012, 34(2): 131-139.
[16] Gu Y, Fang Y, You D, et al. Properties and microstructure of alkali-activated slag cement cured at below-and about-normal temperature[J]. Construction and building materials, 2015, 79: 1-8.
[17] Du J, Bu Y, Cao X, et al. Utilization of alkali-activated slag based composite in deepwater oil well cementing[J]. Construction and Building Materials, 2018, 186: 114-122.
[18] Samantasinghar S, Singh S. Effects of curing environment on strength and microstructure of alkali-activated fly ash-slag binder[J]. Construction and Building Materials, 2020, 235: 117481.
[19] Li P, Tang J, Chen X, et al. Effect of Temperature and pH on Early Hydration Rate and Apparent Activation Energy of Alkali-Activated Slag[J]. Advances in Materials Science and Engineering, 2019, 2019.
[20] Gao X, Yu Q L, Brouwers H J H. Properties of alkali activated slag–fly ash blends with limestone addition[J]. Cement and Concrete Composites, 2015, 59: 119-128.
[21] Xiang J, Liu L, Cui X, et al. Effect of limestone on rheological, shrinkage and mechanical properties of alkali–Activated slag/fly ash grouting materials[J]. Construction and Building Materials, 2018, 191: 1285-1292.
[22] Cheng Q, Tagnit-Hamou A, Sarkar S L. Strength and microstructural properties of water glass activated slag[J]. MRS Online Proceedings Library Archive, 1991, 245.
[23] Temuujin J, Van Riessen A, Williams R. Influence of calcium compounds on the mechanical properties of fly ash geopolymer pastes[J]. Journal of hazardous materials, 2009, 167(1-3): 82-88.
[24] Lee W K W, Van Deventer J S J. The effect of ionic contaminants on the early-age properties of alkali-activated fly ash-based cements[J]. Cement and Concrete Research, 2002, 32(4): 577-584.
[25] Jeong Y, Oh J E, Jun Y, et al. Influence of four additional activators on hydrated-lime [$Ca(OH)_2$] activated ground granulated blast-furnace slag[J]. Cement and Concrete Composites, 2016, 65: 1-10.
[26] Chindaprasirt P, Phoo-ngernkham T, Hanjitsuwan S, et al. Effect of calcium-rich compounds on setting time and strength development of alkali-activated fly ash cured at ambient temperature[J]. Case Studies in Construction Materials, 2018, 9: e00198.
[27] GB/T 17671-1999, Method of Testing Cements-determination of Strength, The State Bureau of Quality and Technical Supervision, Beijing, 1999, p. 9.
[28] Lecomte I, Henrist C, Liegeois M, et al. (Micro)-structural comparison between geopolymers, alkali-activated slag cement and Portland cement[J]. Journal of the European Ceramic Society, 2006, 26(16): 3789-3797.
[29] Qing-Hua C, Sarkar S L. A study of rheological and mechanical properties of mixed alkali activated slag pastes[J]. Advanced Cement Based Materials, 1994, 1(4): 178-184.
[30] Menchaca-Ballinas L E , Escalante-Garcia J I . Low CO_2 emission cements of waste glass activated by CaO and

NaOH[J]. Journal of Cleaner Production, 2019:117992.
[31] Jia Z, Yang Y, Yang L, et al. Hydration products, internal relative humidity and drying shrinkage of alkali activated slag mortar with expansion agents[J]. Construction and Building Materials, 2018, 158: 198-207.
[32] Ravikumar D, Neithalath N. Effects of activator characteristics on the reaction product formation in slag binders activated using alkali silicate powder and NaOH[J]. Cement and Concrete Composites, 2012, 34(7): 809-818.
[33] Haha M B, Le Saout G, Winnefeld F, et al. Influence of activator type on hydration kinetics, hydrate assemblage and microstructural development of alkali activated blast-furnace slags[J]. Cement and Concrete Research, 2011, 41(3): 301-310.
[34] Wang S D, Scrivener K L. Hydration products of alkali activated slag cement[J]. Cement and Concrete Research, 1995, 25(3): 561-571.
[35] Zhu X, Tang D, Yang K, et al. Effect of Ca(OH)2 on shrinkage characteristics and microstructures of alkali-activated slag concrete[J]. Construction and Building Materials, 2018, 175: 467-482.
[36] Ismail I, Bernal S A, Provis J L, et al. Drying-induced changes in the structure of alkali-activated pastes[J]. Journal of Materials Science, 2013, 48(9): 3566-3577.
[37] Kim M S, Jun Y, Lee C, et al. Use of CaO as an activator for producing a price-competitive non-cement structural binder using ground granulated blast furnace slag[J]. Cement and concrete research, 2013, 54: 208-214.
[38] Yang K H , Sim J I , Nam S H . Enhancement of reactivity of calcium hydroxide-activated slag mortars by the addition of barium hydroxide[J]. Construction and Building Materials, 2010, 24(3):241-251.
[39] P. Kumar Mehta, Paulo J.M. Monteiro. Concrete: microstructure, properties, and materials[M]. Prentice-Hall, 2013.
[40] Ye J, Zhang W, Shi D. Setting acceleration and strength enhancement derived from calcium Species for alkali-activated cementitious materials[J]. Journal of the Chinese Ceramic Society, 2017, 45(08):1101-1112.
[41] Wang J, Lyu X J, Wang L, et al. Influence of the combination of calcium oxide and sodium carbonate on the hydration reactivity of alkali-activated slag binders[J]. Journal of cleaner production, 2018, 171: 622-629.
[42] Li, J., Zhang, W., Xu, K., & Monteiro, P. J. (2020). Fibrillar calcium silicate hydrate seeds from hydrated tricalcium silicate lower cement demand. Cement and Concrete Research, 137, 106195.
[43] Jin F, Al-Tabbaa A. Strength and drying shrinkage of slag paste activated by sodium carbonate and reactive MgO[J]. Construction and Building Materials, 2015, 81: 58-65.
[44] Gao X, Yu Q L, Brouwers H J H. Characterization of alkali activated slag–fly ash blends containing nano-silica[J]. Construction and Building Materials, 2015, 98: 397-406.
[45] Collins F, Sanjayan J G. Effect of pore size distribution on drying shrinking of alkali-activated slag concrete[J]. Cement and Concrete Research, 2000, 30(9): 1401-1406.
[46] Kjellsen K O, Detwiler R J, Gjørv O E. Backscattered electron imaging of cement pastes hydrated at different temperatures[J]. Cement and concrete research, 1990, 20(2): 308-311.

Tables and Figures

Table 1. Chemical compositions of GGBS, clinker and CSA (%)

Material	SiO_2	Al_2O_3	CaO	MgO	TiO_2	Fe_2O_3	MnO	SO_3	K_2O	Na_2O	LOI
GGBS	33.04	14.48	37.4	9.63	1.33	0.44	0.2	2.56	0.34	0.27	0.31
PC	23.86	4.76	61.07	2.44	0.36	2.93	0.04	1.09	1.29	0.04	2.09
CSA	10.03	33.25	41.31	1.85	1.42	1.66	0.12	6.89	0.38	0.02	2.57

Table 2. The mix proportions of binders (wt.%)

No	Sample	Slag	Clinker	CSA	$Ca(OH)_2$	$CaCO_3$	CaO	$CaCl_2$
1	AAS (Control)	100	/	/	/	/	/	/
2	AAS-7.5%PC	92.5	7.5	/	/	/	/	/
3	AAS-15%PC	85	15	/	/	/	/	/
4	AAS-6%CSA	94	/	6	/	/	/	/
5	AAS-12%CSA	88	/	12	/	/	/	/
6	AAS-2.5%CH	97.5	/	/	2.5	/	/	/
7	AAS-5%CH	95	/	/	5	/	/	/
8	AAS-7.5%CC	92.5	/	/	/	7.5	/	/
9	AAS-15%CC	85	/	/	/	15	/	/
10	AAS-2.5%CO	97.5	/	/	/	/	2.5	/
11	AAS-5%CO	95	/	/	/	/	5	/
12	AAS-0.25%CCl	100	/	/	/	/	/	0.25
13	AAS-0.5%CCl	100	/	/	/	/	/	0.5

Table 3. Summary of parameters and ages of testing

Type of sample	Samples	Parameters	Age of testing
Mortar	AAS (control), AAS-15%PC, AAS-12%CSA, AAS-5%CO, AAS-0.25%CCl, Pure-CSA	Compressive strength	6 h, 24 h,3 d, 28 d
Paste	AAS (control), AAS-15%PC, AAS-12%CSA, AAS-5%CO, AAS-0.25%CCl, Pure-CSA	Internal temperature changes	1 minute for 24 hours
	AAS (control), AAS-15%PC, AAS-12%CSA, AAS-5%CO, AAS-0.25%CCl	XRD, TGA, MIP	6 h, 28 d
	AAS (control), AAS-15%PC, AAS-12%CSA, AAS-5%CO, AAS-0.25%CCl	BSE	6 h

Note: Pure-CSA refers to the binder was CSA alone as the reference sample, and water was added to give 0.35 W/B, instead of alkali solution.

Table 4. The pore size distribution ratio of AAS paste curried at 6 h and 28 d

Sample	6 h (%)					28 d (%)			
	<0.01 μm	0.01-0.03 μm	0.03-5 μm	>5 μm		<0.01 μm	0.01-0.03 μm	0.03-5 μm	>5 μm
AAS-15%PC	17.29	70.77	6.54	5.40		64.65	31.15	0.80	3.40
AAS-12%CSA	15.81	77.58	3.86	2.75		55.86	41.43	0	2.71
AAS-5%CO	21.98	58.58	9.95	9.49		66.55	24.22	6.07	3.16
AAS-0.25%CCl	14.53	74.90	7.04	3.53		70.20	24.16	2.54	3.10
AAS (control)	18.46	74.82	4.45	2.27		75.92	20.53	1.52	3.03

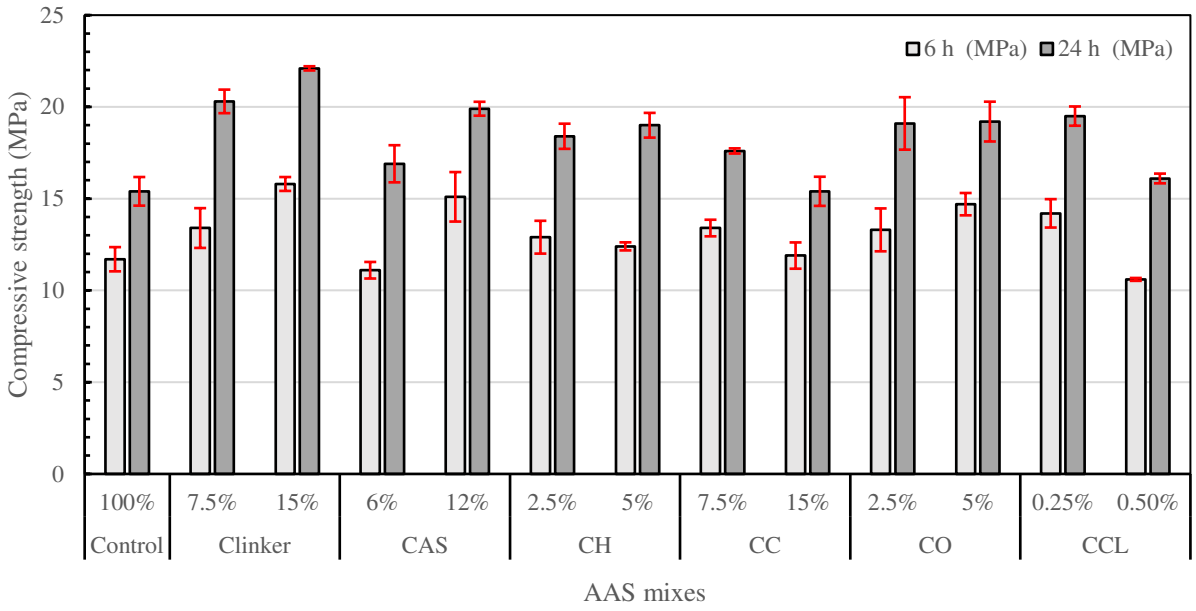

Fig. 1. Effect of calcium-rich materials on early strength of AAS mortar under low temperature environment (5 ºC)

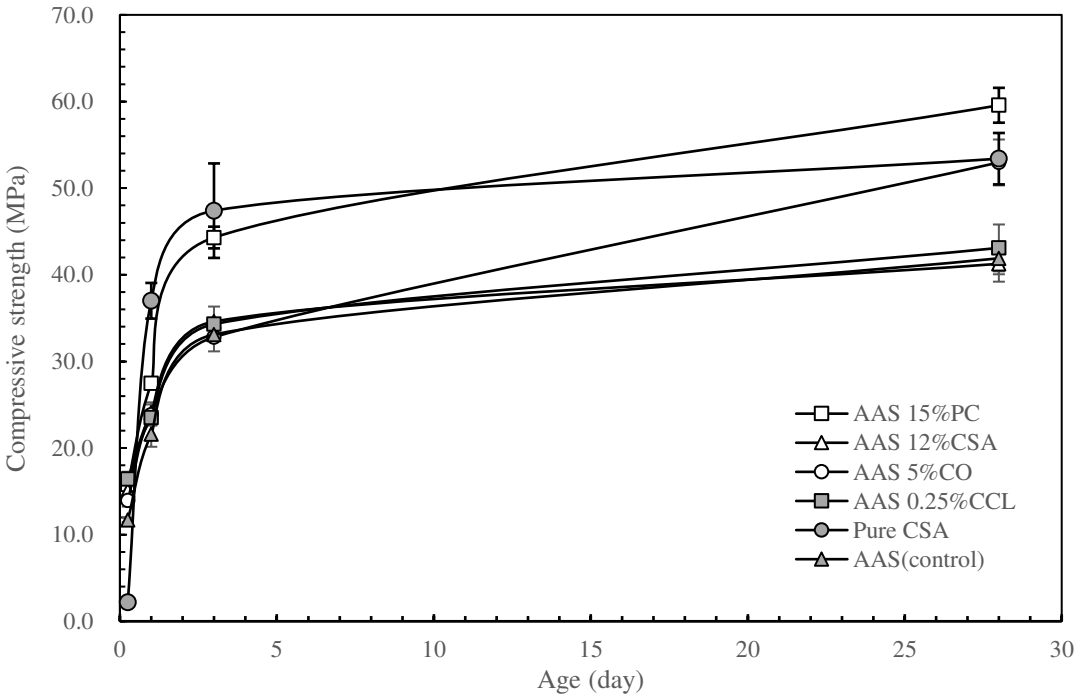

Fig. 2. Effect of calcium-rich materials on the compressive strength of AAS mortar (W/B = 0.35)

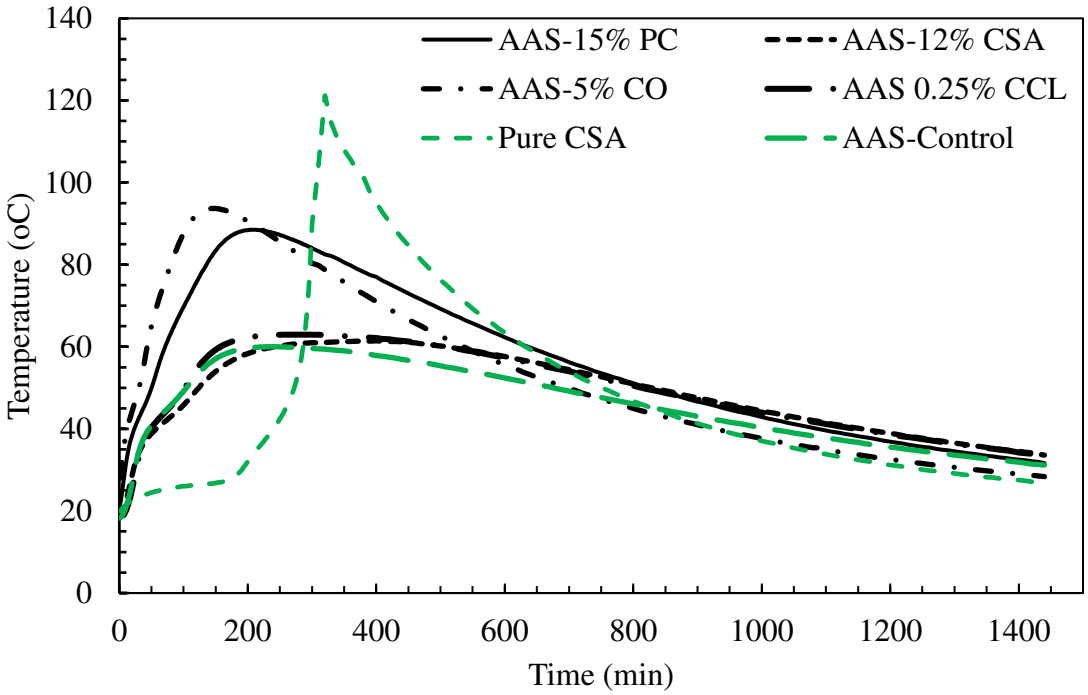

Fig. 3. Internal temperature change of paste at early age

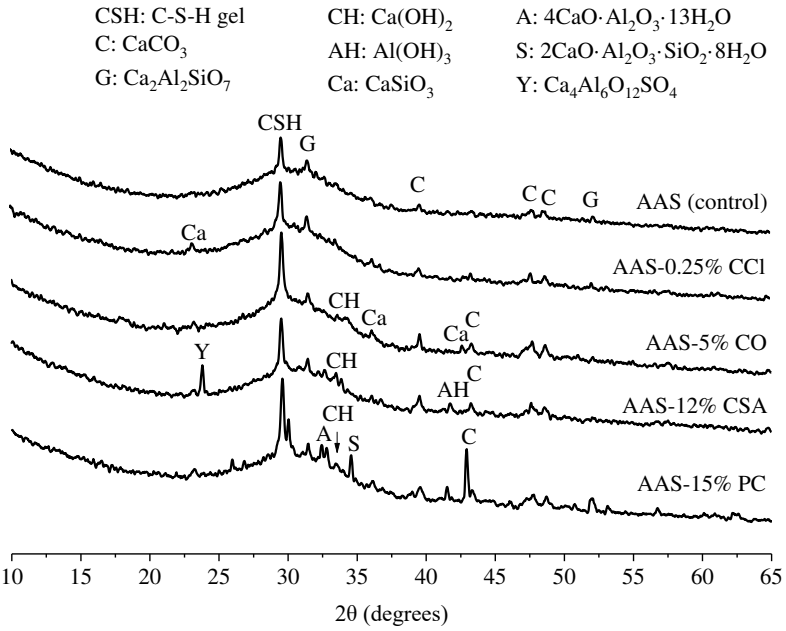

a (6 h)

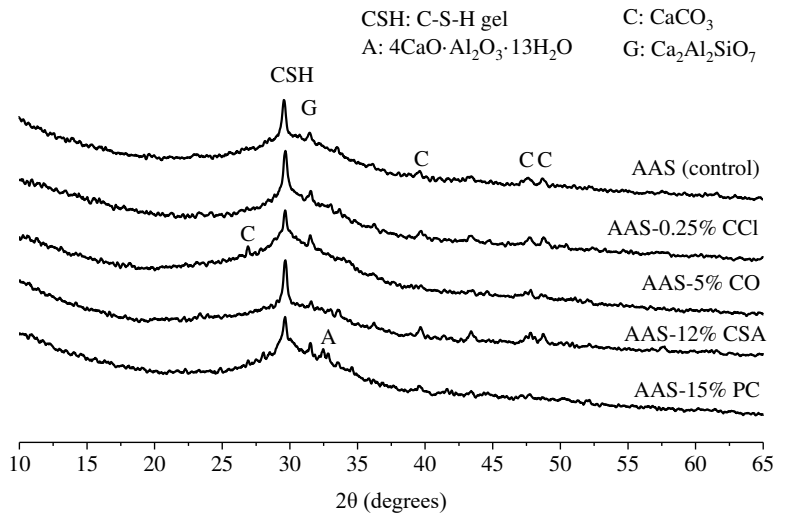

b (28 d)

Fig. 4. XRD patterns of AAS pastes at 6 h (a) and 28 d (b)

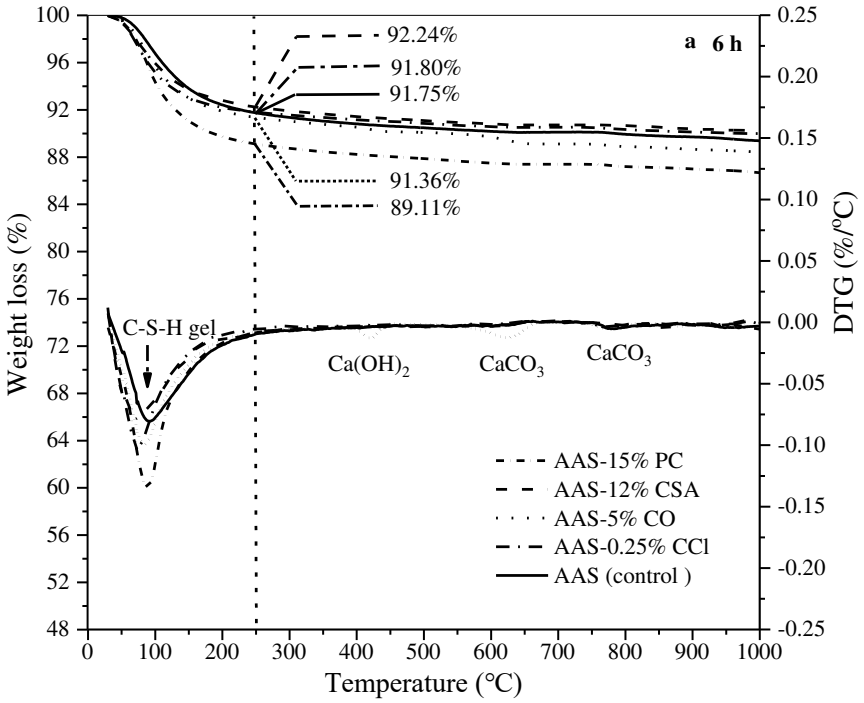

521

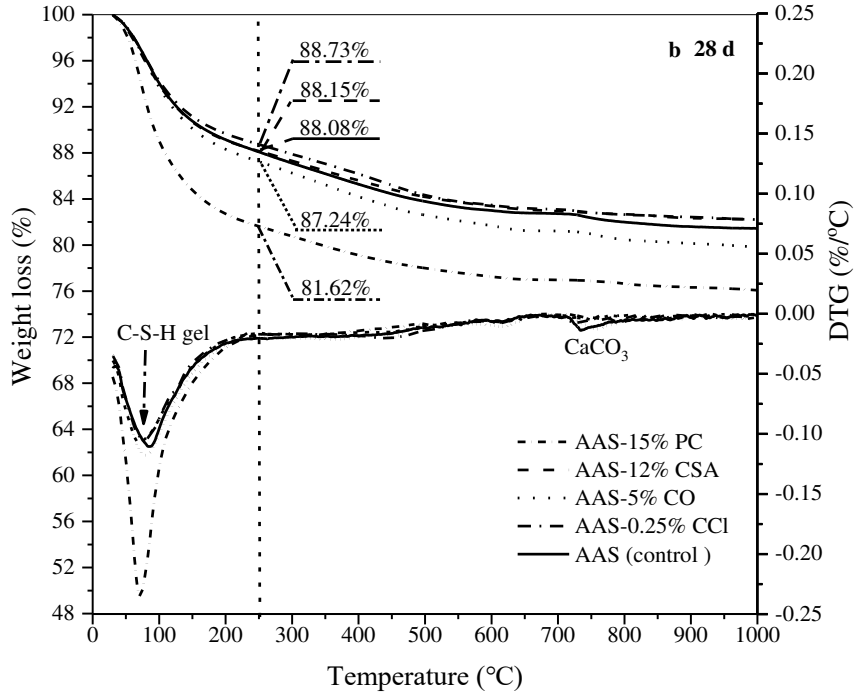

522

523 **Fig. 5.** TG/DTG results of AAS pastes at 6 h (a) and 28 d (b)

524

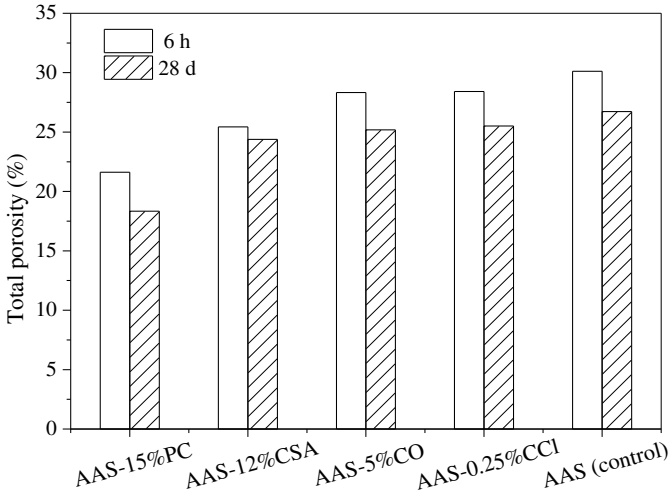

525
526 **Fig. 6.** Total porosity of AAS paste cured at 6 h and 28 d
527
528

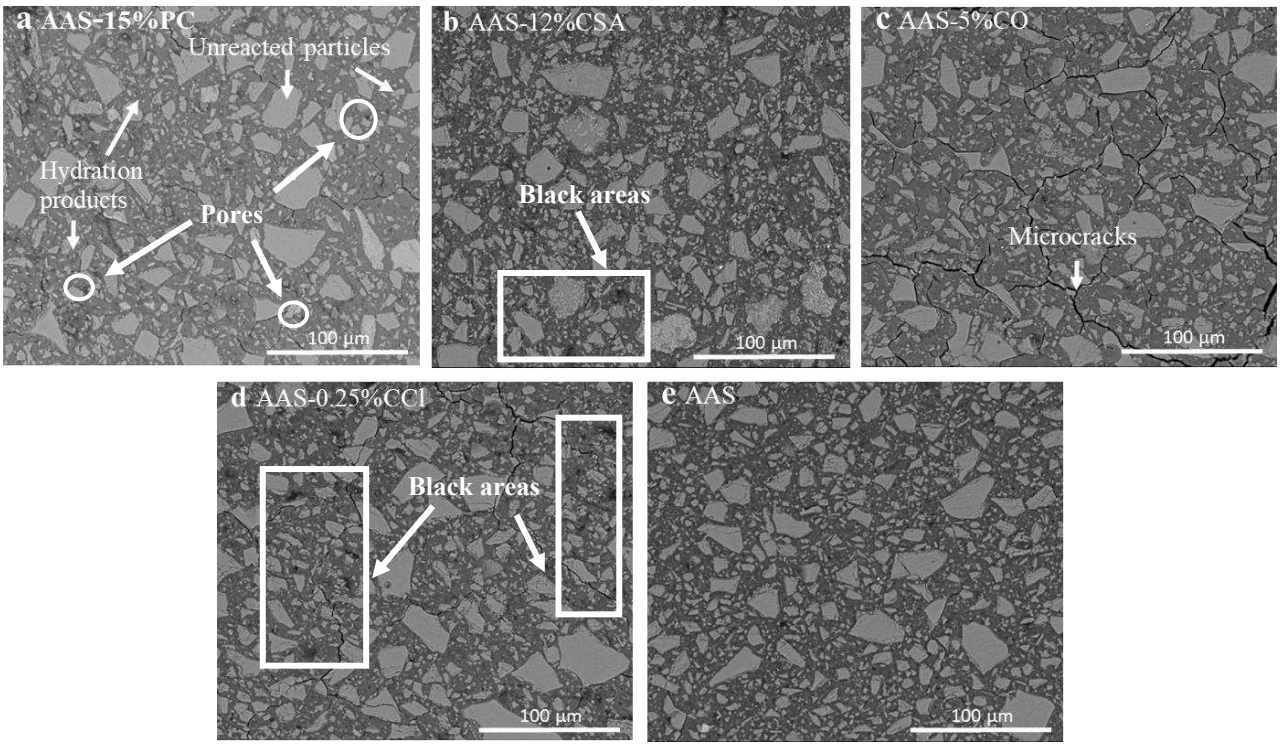

529
530 **Fig. 7.** BSE images of AAS samples with calcium-rich material curing at 5ºC after 6 h
531

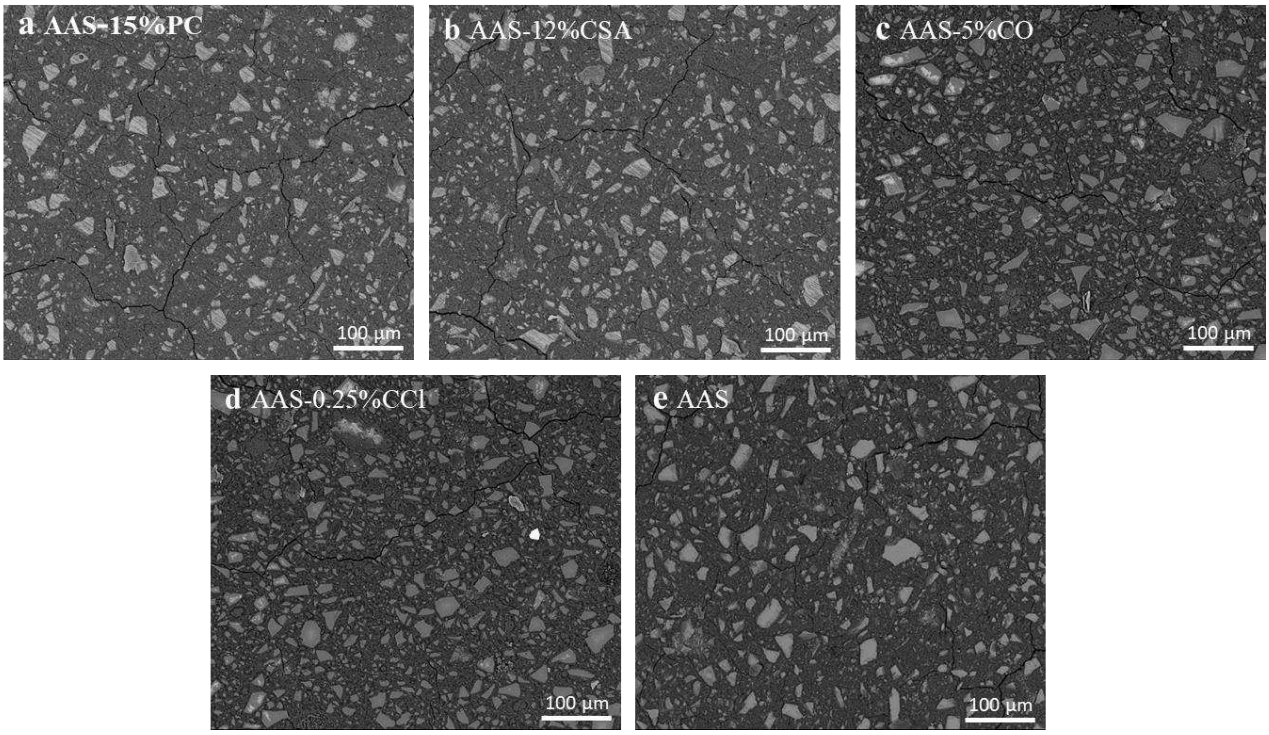

532
533 **Fig. 8.** BSE images of AAS samples with calcium-rich material curing at 5ºC after 28 d
534